Proceedings of the International Association for Shell and Spatial Structures (IASS) Symposium 2009, Valencia
Evolution and Trends in Design, Analysis and Construction of Shell and Spatial Structures
28 September – 2 October 2009, Universidad Politecnica de Valencia, Spain
Alberto DOMINGO and Carlos LAZARO (eds.)

Influence of various types node connectors on the buckling loads of grid shells

Kyung-Ju HWANG*, Jan KNIPPERS[a], Sun-Woo PARK[b],

*Researcher, Institute of Building Structures and Structural Design, University of Stuttgart
Keplerstrasse 11, 70174 Stuttgart, Germany
k.hwang@itke.uni-stuttgart.de

[a] Professor, Institute of Building Structures and Structural Design, University of Stuttgart
[b] Professor, The Korean National University of Arts

Abstract

Node connectors used in grid shells have various geometrical characteristics, which makes it difficult to compare them. Moreover, since free-form spatial structures have been introduced in the field of architecture, optimal connector design has become one of the crucial points for the stability of global structure. This paper presents the influence of various node connecting systems on the buckling loads of grid shells. The authors, at first, selected and investigated four connecting systems displaying different geometrical characteristics which are adapted in normal grid shells and free-form spatial structures. Using nonlinear beam elements with nonlinear spring elements in the commercial FEA package ANSYS, three-dimensional FE tests of node connectors were performed, taking into particular consideration the parameters of differing bolt clearances in the joint to estimate the ultimate loading capacities. The effects of moment-rotation and axial force were transferred to nonlinear spring elements on the grid shells. In conclusion, the results present the influence of bolt clearances of node connectors with geometrical imperfection on the buckling loads of grid shells.

Keywords: Bolt clearance, node connector, semi-rigid joint, geometrical imperfection, free-form spatial structure, grid shell

1. Introduction

Many researchers have already reported that the stiffness of connecting systems plays a very important roll in the structural behavior of spatial structures. Additionally, the assembling and geometrical procedure of connecting systems should be well accommodated to save cost and construction time. To provide a proper connecting system

for the spatial structure considering both structural and geometrical characteristics, companies and researchers have suggested various types of node connecting systems with very different geometrical and structural features. Since free-form spatial structures have appeared in the field of architecture, even more types of connectors have been developed for use in practice. In terms of the design of single-layer grid shells, so far most analysis of connection behaviors has been assumed to be either of a perfect pinned or rigid joint. However, most real node connecting systems in spatial structures are neither a perfect pinned nor a perfect rigid joint, but a semi-rigid connection which shows nonlinear stiffness behavior. Most of all, unplanned deviation of the bolt-holes may bring more severe nonlinear characteristics, so that the load bearing capacity of node connectors may be weakened.

As for the deviation of bolt-holes in the steel structure, the European standard prEN 1090-2 very simply mentions the available application of bolt-holes, but that is not enough to estimate exact structural integrity between deviations of bolt holes in the node connector and the whole spatial structure (Hoelbling et al [9]). Thus, it is significantly necessary to investigate the influence of node connectors, taking deviation of the bolt-holes on the grid shell structure into consideration.

2. Numerical investigations of four node connectors

To investigate the characteristics of various geometrical forms of node connectors while considering different deviations of bolt-holes, four node connectors are introduced which have been used in spatial structures and free-form grid shells, meaning the main characteristics of the systems are comparable to the real one.

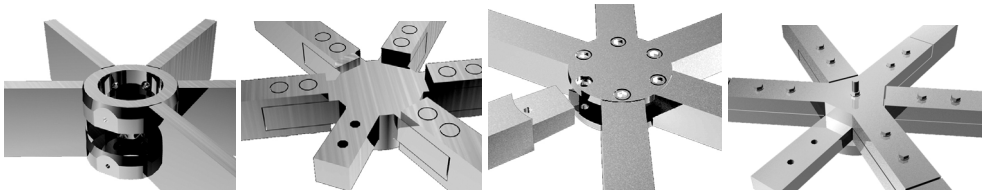

System 1 System 2 System 3 System 4

Figure 1: The four node connector models

2.1 Geometric details of the test

Figure 1 presents the models of four node connectors. System 1 consists of two dish nodes, to which beam members are connected by two screw threads. System 2 is assembled with a solid plate as node with 6 horizontal finger splice plates. The ends of the beam members were fabricated as fork-form fittings, which can be connected to the finger splice plates of the node by two or more counter-sunk bolts in double shear. The third node connecting system consists of two flat discs with a circular groove. The beam members are fitted with shear tongues which are then inserted into the grooves of the two discs. The discs and the beam member are connected by bolts. As for system 4, two flat plates are connected by a

single central bolt. Each beam member is connected to the horizontal splice plates by two bolts in single shear plane (Stephan et al [7]).

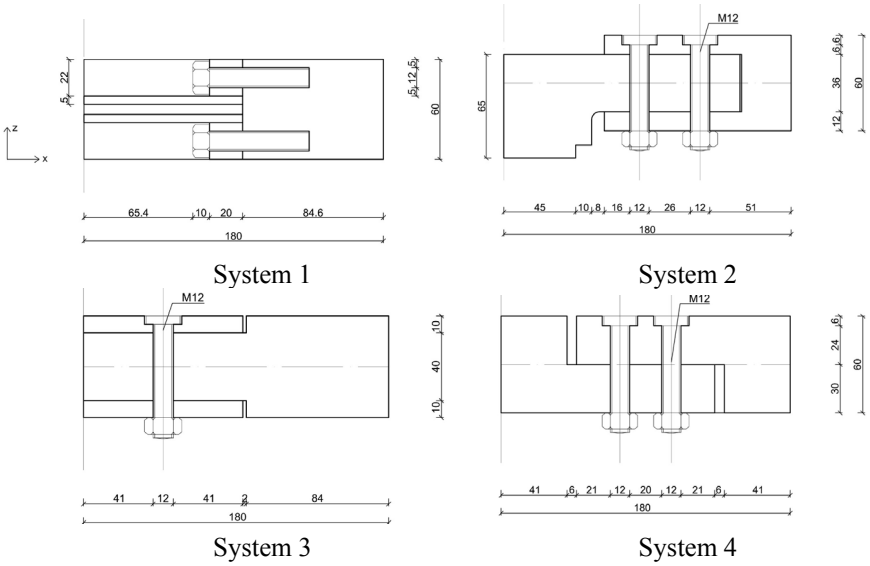

Figure 2: Details of four node connectors used in numerical simulation

As shown in Figure 5, two bending tests (My, Mz) and an axial test (N) were performed. Although each model has different geometries, the length (L) of all specimens was assumed to be 180 mm with a cross section b×h=60mm×60mm. Especially, in order to consider the influence of differing sizes of bolt-holes, two parameters for the deviation of bolt-holes (ΔV), 0.1mm and 2.0mm, were adopted to systems 2, 3 and 4 (Figure 3). The ΔV of system 1 was assumed as 0, because the bolt connection in system 1 was assumed to be the screw thread type.

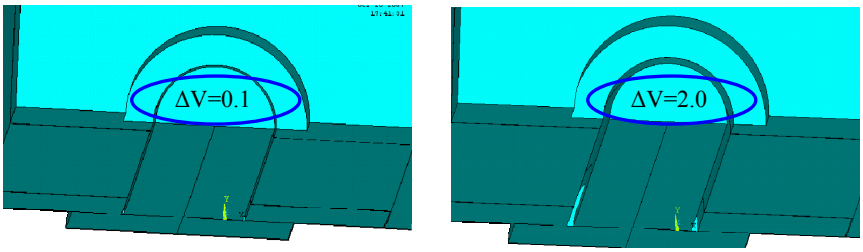

Figure 3: Deviation of bolt holes (ΔV) in the node connector (mm)

2.2 The Finite Element Model

In the finite element model, all elements of the beams, bolts and node were meshed by the 10-node tetrahedral solid structural elements SOLID 92. The important interfaces between node and end of beam as well as the surfaces of bolts were simulated by creating contact pairs with the 3-D target surface element TARGET 170 and the 3-D 8-node surface-to-surface contact element CONTACT 174. To reduce the number of contact planes, the bolt head or nut and beam element for the bending test around the y-axis (My) are assumed to be fully connected. This simplification may lead to somewhat stiffer deformation, however the overall behaviour is not greatly influenced, as already mentioned in the references (Coelho et al [2]) For the bending test around z-axis(Mz) and axial force test(N), the bolt head and beam element could be separated. Due to their geometrical symmetry about the central axis a one-half symmetrical model has been used to save computation time.

2.3 Material properties

At first, all the material is assumed to be steel S355, giving a yield strength and elastic modulus of 355 N/mm² and 210000 N/mm², with a Poisson's ratio 0.3, respectively. In order to simplify for plastic behavior, the stress-strain relationship for node and beam was taken as elastically-perfect plastic. Because the high strength bolts included the bolt head and nut, Figure 4 shows that the stress-strain curve was applied as a trilinear, with the defining points that have been introduced in other similar literature (Shi et al [3]). The coefficient of friction for the contact surface between node and beam was taken as 0.3.

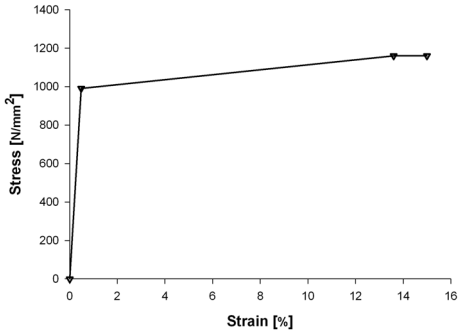

Stress (N/mm²)	Strain (%)
0	0
990	0.483
1160	13.6
1160	15

Figure 4: Stress-strain curve for high strength bolts (Shi et al [3])

2.4 Loading and boundary condition

The setup for the numerical models is a symmetric cantilever arrangement. In the symmetry plane xz, the nodes for bending test My and axial test N could be fixed with symmetric geometric boundary conditions. However, the xy plane can not meet such a symmetrical condition, since the bolt elongation behavior of Mz is not symmetrical along xz plane. In terms of the load of bending, as shown in Figure 5, the end of the node element is fixed and the displacement loading was applied at the end of the beam element. To obtain the axial force, axial displacement loading was applied at the end of beam. Figure 5 shows the

definition of moment-rotation relation and load-displacement of axial force tests which have been introduced in other literature related to steel beam-column behavior (Gebbeken et al [6]). To obtain a more specialized anaylsis, a specific analysis tool or formula for each case of node connector type may be needed, using the same conditions respectively. However, the most significant characteristic of the node connector is the overall behavior of load-displacement relationship (Coelho et al [2]), so that the influence of node connector capacity on the global grid shell can be investigated. This paper thus made use of a simplified definition of bending and axial stiffness.

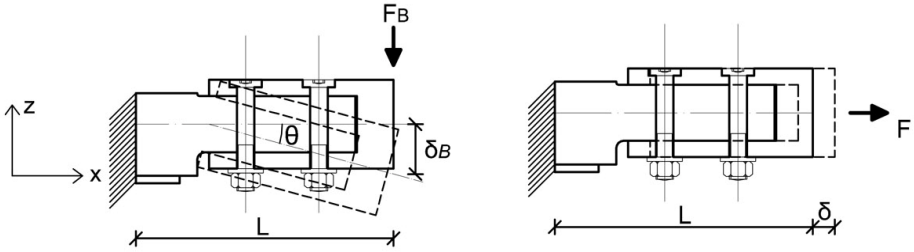

Figure 5: Definition of moment-rotation relationship and axial load and displacement

The corresponding moment (M) is the product of FB with the distance L.

$$M = F_B \times L \tag{1}$$

The definition of rotation θ is given that the displacement δB is divided by the length (L).

$$\tan\theta = \frac{\delta_B}{L} \approx \theta \text{ for } |\theta| < 1 \tag{2}$$

2.5 Numerical results

In the above selected numerical models, bending (My and Mz) and axial tension tests were performed. Figure 6 and 8 show moment-rotation and load-displacement curves for each model using two different parameters for bolt clearance: 0.1mm and 2.0mm. In each simulation test, the rotation of the joint relative to the node and beam connection is determined from the displaced shapes of node connectors. As mentioned, system 1 is assumed to be fully connected between bolt and beam, thus the moment-rotation curves of My and Mz show very stiff behavior. Moreover, node and beam are connected without discontinuity which leads a loading transfer well. System 2 and System 4 present very interesting differences influenced by the shapes of connecting systems. System 2 has a fork-shaped beam end with two shear planes; tension and compression stresses can be transferred to the beam through two shear planes very effectively. The stress distribution of system 4 is not effective because the connections use an L-shaped node and beam attached by only one shear plane, so that almost half of the node can transfer bending stress (Figure 7). Thus, for example, the bending stiffness My of system 4 (ΔV =0.1) is around 50% less than that of system 2.

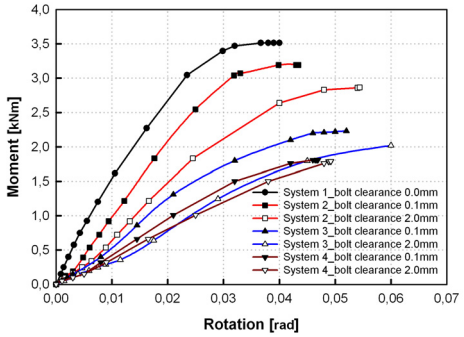

(a) My

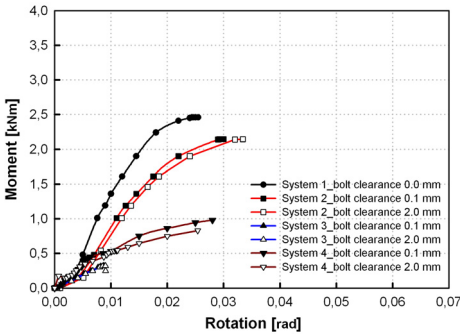

(b) Mz

Figure 6: Moment-rotation curves of four node connectors

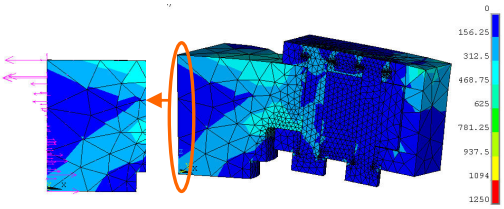

(a) System 2

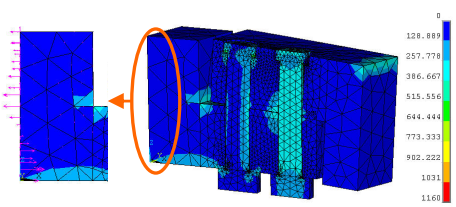

(b) System 4

Figure 7: Von Mises stresses and reactions' distributions of system 2 and 4

In relation to bolt clearance ΔV, they show a different mode of behavior. Although the geometrical shape of system 4 caused less stiffness than system 2, the unsymmetrical form with one shear plane was not as influenced between ΔV=0.1 and 2.0mm, because the upper and lower parts of the fork-shaped beam ends of system 2 should move simultaneouslly with tensial and compressive load.

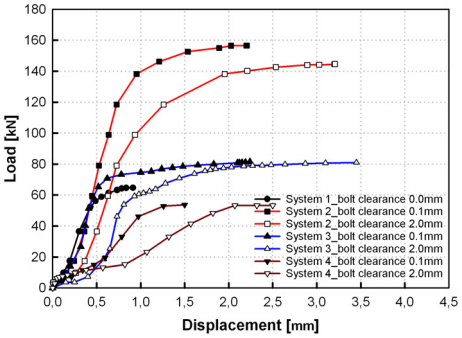

Figure 8: Load-displacement curves of axial loading tests

However, the L-shaped node and the beam end of system 4 would transfer the load to the node as prying force, so that the rotation of connector with a larger bolt-hole (ΔV=2.0) was restrained. As shown in Figure 6, bending stiffness (My) of system 4 with ΔV=2.0 was only 5.4% lower than the case of ΔV=0.1, while system 2 showed about a 22% difference between ΔV=0.1 and 2.0. As for the results of axial test (N), most of the curves show that plastic bearing of the bolt could compensate for the deviation of bolt-holes, and they have similar strength of axial force to each other, even though the stiffness of ΔV=0.1 is generally higher than that of ΔV=2.0 (Figure 9).

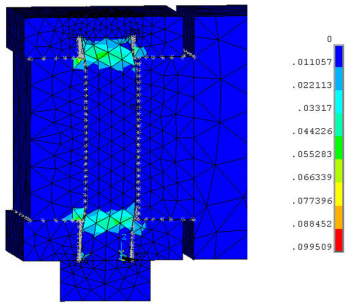

	$N_{a,R,k}$ = 60 kN	N_u = 80 kN
ΔV (mm)	ε1 (%)	
0.1	0.90	5.19
2.0	3.30	9.95

Figure 9: Plastic principal strain ε1's distribution of system 3 at the ultimate load and principal plastic strain at the characteristics shear forces ($N_{a,R,k}$) and at the ultimate shear forces N_u of system 3

3. Influence of various node connectors on the global grid shells

Using the all of moment-rotation curves and load-displacement curves which were performed in Chapter 2, the predicted influence of different nodal stiffness due to deviations of bolt-holes (ΔV) in the joints was applied to the global grid shells.

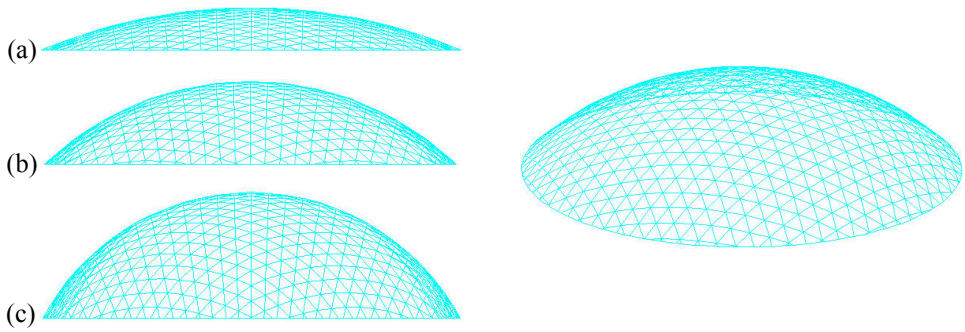

Figure 10: Models of three way grid dome

As shown in Figure 10, the three way grid dome with a span of 25m was simulated using three different ratios of rise (f) to span (d) [0.1(a), 0.2(b) and 0.3(c)] to find out the overall behavior of the global grid shells with different rise-span ratios (f/d) and ΔV. The material of the beam element was assumed to be steel S355 with E-Module 210000 N/mm². The cross section was b×h=60mm×60mm and the length of beam (L) was 1.20m. For the boundary condition, the rigid support was adopted. The dead load (g) of steel beam was γ=78.5 kN/m³ and 20 mm thickness of glass glazing (γ=25 kN/m³) was calculated as well. As for the live load, a snow load (s) of 0.75 kN/m² was applied to the structure.

To obtain a critical point in the load-carrying characteristic of the dome, the load control method was performed. According to the German standard DIN 18800, the design load factor (p) was incremented from p=1.35g+1.5s, corresponding to loading factor 1.0 (Knippers et al [5]). Concerning to the load cases, a symmetrical load case g+s and asymmetrical load case g+s/2 were applied to the structures. The initial geometric imperfection vector was obtained by linear combination of eigenvectors at the critical point of the load-displacement curve and then the scaling of 50 mm was sized to the first eigenmode. All of the critical failure was assumed to have occurred in the global area assuming no member buckling took place, in order to find out the influence of nodal stiffness on global instability behavior. For that the strength of cross section was checked through a postprocessor using the condition: [Bulenda et al (8)]

$$\frac{M_y}{M_{y,pl,d}} + \frac{M_z}{M_{z,pl,d}} + \left(\frac{N}{N_{pl,d}}\right)^2 \leq 1 \tag{3}$$

with N, M_y and M_z : internal forces from the elastic computation and $N_{pl,d}$, $M_{y,pl,d}$ and $M_{z,pl,d}$: limit state yield forces at design load level by post-processors.

3.1 Finite Element Models

Figure 11 shows the elements that were used in the finite element model. To consider both geometric and material nonlinearities in the grid shell with a semi-rigid connection, three nonlinear spring elements of COMBIN39 supported by a particular function of ANSYS were implemented to simulate nodal stiffness.

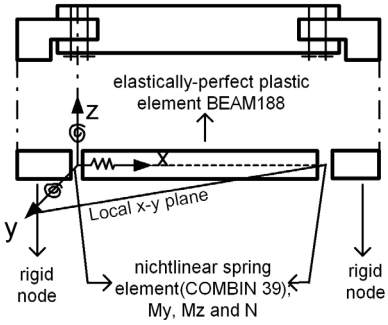

Figure 11: Finite element applied in grid shells

This element is a nonlinear spring element which has a unidirectional degree of freedom. In this analysis, the bending stiffness (My and Mz) and axial force (N) could be simulated by inputting the real constants of COMBIN39. The center of node and beam were simulated by BEAM188 and the node was assumed to be a rigid body. In order to ensure the physical behavior of nonlinear spring elements at the node, a local coordinate system was necessary to all elements (Ma et al [4]).

3.3 Results of parameter study

3.3.1 The influence of rise-span ratio and nodal stiffness on buckling load

Based on the moment-rotation and load-displacement curves of four node connectors in Figures 6 and 8, the global grid shells were investigated with three rise-span ratios (f/d=0.1, 0.2 and 0.3). Figure 12 shows the failure load factors related to f/d and node connecting system (ΔV=2.0). As shown in Figure 12, general failure load factors increase with the increment of the rise-span ratios and the node connector system, which has a high nodal stiffness with high rise-span ratio, draws near to the failure load factor of the rigid connecting system. The influence of node connector stiffness with geometric initial imperfection shows clearly for the high-rise dome. For example, the perfect system with system 4 in f/d=0.3 presents about 2.5 times higher failure load factor than the initial imperfection one. In case of f/d=0.1, most of models show a low failure load factor, and all of the models using systems 1 to 4 could not even reach design load level (p=1).

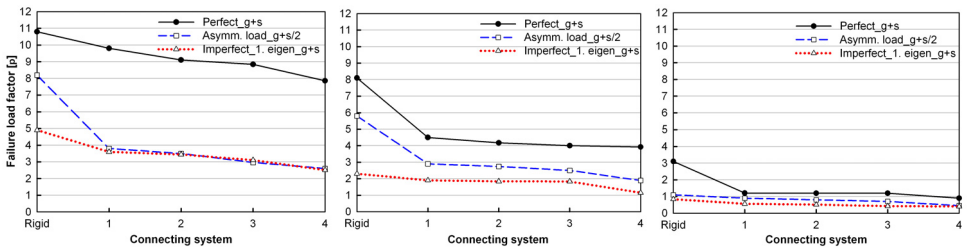

(a) f/d=0.3 (b) f/d=0.2 (c) f/d=0.1

Figure 12: Failure load factor (p) – f/d and node connecting systems (ΔV=2.0)

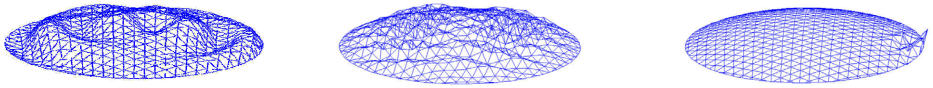

(a) Rigid connection (b) Connector system 1 (c) Connector system 4

Figure 13: First eigenmode of grid shells – f/d=0.1(ΔV=2.0)

The low failure load factor obtained by a combination of low stiffness of connection type and initial imperfection in a low rise-span ratio can also be observed in the stress distribution. As shown in Figure 14, by increasing external force, a non-uniform stress

occurred easily in the model, thus geometric imperfection of the dome along with a low stiffness of connection type in a low rise-span ratio causes the membrane stress to easily switch to bending stress, leading to buckling behavior in the dome.

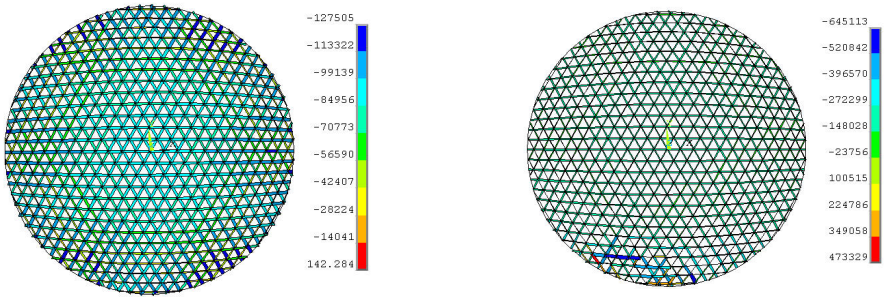

(a) before buckling (b) after buckling

Figure 14: Member forces of grid shell – f/d=0.2 with node system 4 (ΔV=2.0)

This buckling tendency can also be seen in the model f/d=0.2. Figure 15 shows the load-displacement behavior of the grid shell f/d=0.2 and the form resistance, with membrane stress changing to bending stress with the low nodal stiffness in the initial imperfection as easily as with f/d=0.1. However, even though the grid shells are connected with a low stiffness type of joint, the perfect systems show different paths of buckling failure. For instance, the failure load factor of perfect geometry with the weakest node type system 4 increases until factor 3 before the bifurcation occurred in the model.

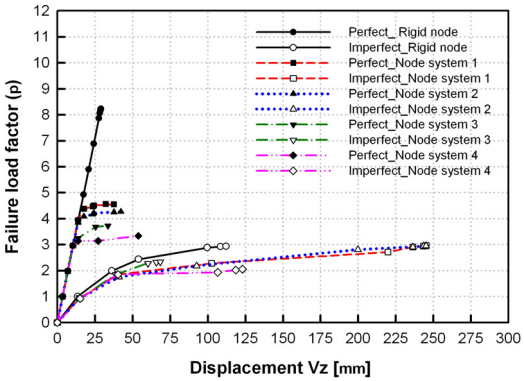

Figure 15: Load-displacement curves of grid shell – f/d=0.2 (ΔV=2.0), load case g+s

3.3.2 The influence of different bolt clearances on buckling load

Figure 16 shows the failure load factors of grid shells concerning bolt clearances ΔV. With the high rise model such as f/d=0.3, a more obvious difference in failure load factor could

be observed than with the model using connected node system 4, because the stiffness of node system 2 shows more clear differentiation than the node system 4. However, as shown in Figure 16(b) and (d), the influence of node types shows very small differences between systems 2 and 4. As may be expected, the global buckling of the low rise-span is dominant, so that the stiffness of node system may not play a significant roll in buckling behavior. In spite of that, ΔV=0.1 of node system 2 with initial imperfection obtained a failure load factor 1.15 which is factor 0.5 more than ΔV=2.0, because My of ΔV=0.1 in system 2 was around 35% higher than ΔV=2.0. In the case of node system 4, even though a high-rise shell was performed, the load factor of ΔV=0.1 with imperfection and load case g+s/2 shows almost same value, because the bending stiffness My and Mz between ΔV=0.1 and 2.0 of system 4 are almost the same.

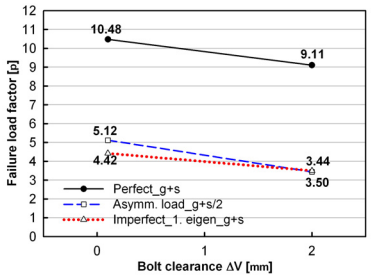

(a) f/d=0.3-Node system 2

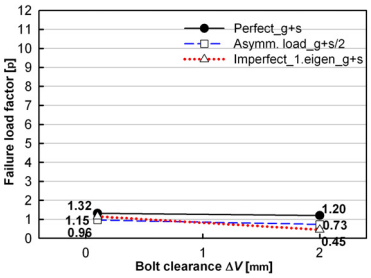

(b) f/d=0.1-Node system 2

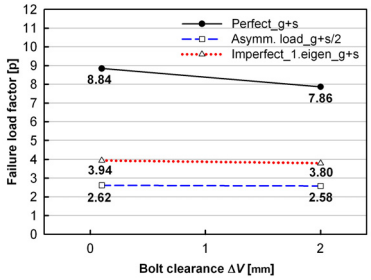

(c) f/d=0.3-Node system 4

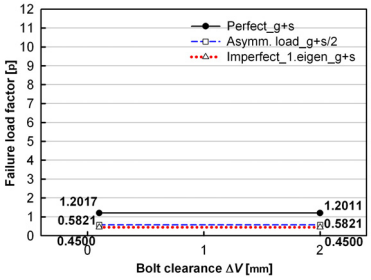

(d) f/d=0.1-Node system 4

Figure 16: Failure load factors with bolt clearances

4. Conclusions

To achieve the purpose of this paper, determining the influence of buckling load with different size of bolt holes of node connectors in global grid shells, finite element analysis with four node connecting systems suggested that the influence of bolt clearances in grid shells could be investigated through instability analysis of 25m three way grid dome, which was performed with different nodal stiffness taking differing bolt-hole sizes into consideration.

First, finite element analysis of the four node connectors presents that different shapes of joint determine the varying stiffness of node systems. Generally speaking, the node connectors which have two shear planes showed higher stiffness than those with one shear plane. On the other hand, the node connector which was connected with an unsymmetrical beam end with one shear plane was not as influenced by different bolt-holes as those using two shear planes because of the shape of the joint assembly. Secondly, low nodal stiffness in conjunction with initial geometrical imperfection leads membrane stress to change to bending stress easily, so that the critical point of grid shell occurred at a low failure load factor. The influence of different bolt clearances in a grid shell depends mainly on the node stiffness and rise-span ratio. In a high-rise perfect grid shell with system 2, the load factor with ΔV=0.1mm obtained around 13% higher than ΔV=2.0mm. System 4 with same rise-span ratio presented around 12% difference because axial forces(N) of both of systems showed different stiffness. However, the imperfection shell using system 4 showed almost no difference, because the bending stiffness of system 4 had little difference in stiffness between ΔV=0.1 and 2.0mm. Thus, the overall structural behavior of an imperfect high-rise grid shell can be very sensitive, displaying a large deviation in bending stiffness due to bolt clearances.

References

[1] A.M. Harte and D.M. Cann, Finite element modelling of the semi-rigid behaviour of pultruded FRP connections, *Journal of Materials Processing Technology*, 2001, 119, 98-113.

[2] G. Coelho, L. S. Silva and F. S. K. Bijlaard, Finite-Element Modeling of the Nonlinear Behavior of Bolted T-Stub Connection, in *ASCE 2006. Journal of Structural Engineering*, June 2006, 918-928.

[3] G. Shi, Y. Shi, Y. Wang and M. A. Bradford, Numerical simulation of steel pretensioned bolted end-plate connections of different types and details, *Engineering Structures,* February 2008.

[4] H. H. Ma, F. Fan and S.Z. Shen, Numerical parametric investigation of single-layer latticed domes with semi-rigid joints, in *IASS 2008, Journal of the International Association for Shell and Spatial Structures*, Vol. 49, 2008, 99-110.

[5] J. Knippers, T. Bulenda. and M. Stein, Zum Entwurf und zur Berechnung von Stabschalen, *Stahlbau*, 1997; 66; 31-37.

[6] N. Gebbeken, B. Binder and H. Rothert, Zur numerische Analyse von Kopfplatten-Verbindungen, *Stahlbau*, 1992; 61; 265-274.

[7] S. Stephan, J. Sanchez-Alvarez and K. Knebel, Reticulated Structures on Free-Form Surfaces, *Stahlbau*, 2004; 73; 562-572.

[8] T. Bulenda and J. Knippers, Stability of grid shells, *in Computers and Structures 79*, 2001, 1161-1174.

[9] W. Hoelbling, T. Misiek and H. Saal, Tragverhalten von Schrauben in Scher-Lochleibungs-Verbindung mit ungenau hergestellten Schraubenlöchern, *Stahlbau*, 2009; 78; 42-46.